Check for updates

AGU ADVANCING EARTH AND SPACE SCIENCES

Space Weather

RESEARCH ARTICLE
10.1029/2026SW004959

Importance of High Cadence Magnetometer Data for Investigating Geomagnetic Disturbances

G. E. Bower[1], S. M. Imber[1], S. E. Milan[1], C. Beggan[2], and J. W. Gjerloev[3]

[1]School of Physics and Astronomy, University of Leicester, Leicester, UK, [2]British Geological Survey, Edinburgh, UK, [3]Johns Hopkins University Applied Physics Laboratory, Laurel, MD, USA

Key Points:

- Geomagnetic disturbances (GMD) occur on different timescales of hours, several minutes and tens of seconds
- 1-s cadence magnetometer data consistently records higher geomagnetic disturbance amplitudes particularly at low geomagnetic latitudes
- Higher than 1 min cadence is important for the 17-03 magnetic local time sector

Correspondence to:

G. E. Bower,
geb23@leicester.ac.uk

Citation:

Bower, G. E., Imber, S. M., Milan, S. E., Beggan, C., & Gjerloev, J. W. (2026). Importance of high cadence magnetometer data for investigating geomagnetic disturbances. *Space Weather*, *24*, e2026SW004959. https://doi.org/10.1029/2026SW004959

Received 21 JAN 2026
Accepted 28 MAY 2026

Author Contributions:

Conceptualization: S. M. Imber, S. E. Milan, C. Beggan
Data curation: J. W. Gjerloev
Formal analysis: G. E. Bower
Funding acquisition: S. M. Imber
Methodology: G. E. Bower, S. M. Imber, S. E. Milan
Supervision: S. M. Imber, S. E. Milan
Visualization: G. E. Bower
Writing – original draft: G. E. Bower
Writing – review & editing: S. M. Imber, S. E. Milan, C. Beggan, J. W. Gjerloev

Abstract Geomagnetic disturbances (GMDs) are rapid changes in the magnetic field of the Earth that may drive geomagnetically induced currents (GICs), known to cause damage to infrastructure such as power grids and pipelines. Globally, GIC measurements are often hard to obtain; therefore, GMDs are used as a proxy for GICs. GMDs have been previously shown to occur on different timescales which are related to different formation mechanisms such as magnetic storms, substorm activities and sudden commencements. 1 min cadence ground-magnetometer data has been available for decades and are the basis of many studies showing the frequency and intensity of GMDs. In recent years one-second cadence data have become available from a network of magnetometers through the SuperMAG portal. We take the 1-s data, averaged 10 s data, and compare the number of GMDs identified with the number found from the 1-minute data to test the GMDs related to the different timescales. We find that 1-s data consistently record higher amplitude GMDs as well as recording overall more GMDs, thus showing the importance of 1-s cadence data. This is most important for GMDs between 00 and 03 magnetic local time and at low geomagnetic latitudes (>50°) as these are the locations where difference between the number of GMD detections between the 1-s data and the 1-min data is the largest. However, the 1-s data have many artefacts due to unreliable data points in them leading a 10-s median being more reliable at correctly detecting GMDs.

Plain Language Summary Rapid changes in the magnetic field of the Earth can lead to excess currents flowing through infrastructure such as power grids and pipelines which can lead to a loss of service and impact society. The rapid changes can be measured by ground magnetometers. For many years data have been recorded at 1 min cadence and this has been the basis for multiple studies. Since 2010 however one-second cadence data have become more widely available. We investigate the number of rapid changes identified in the 1 s data and compare with the number found from the same station in the minute data as well as in a 10 s average. We find that the 1 s data consistently records higher magnitude rapid changes in the magnetic field showing the advantage of 1 s data. We also show that the 1 s is of most importance at magnetic latitude below 50° and in the post-midnight magnetic local time sector. Although the 1 s data contain many artefacts, which are removed in 10 s median data and as such 10 s data currently provided the best trade-off.

1. Introduction

By Faraday's law a geoelectric field can be induced in the surface of the Earth when there are rapid changes in the magnetic field, causing currents to flow where there is a gradient in the potential. These currents are called geomagnetically induced currents (GICs) and are known to cause damage to infrastructure. The impact of GICs has become more important as we become more dependent on infrastructure that is susceptible to failure under large GIC such as power lines and pipelines (Albertson et al., 1973; Campbell, 1978; Marshall et al., 2010). The most famous example of such failures is the Hydro-Quebec blackout on 13th March 1989 where there was a collapse of the power system due to a large geomagnetic storm which required the replacement of multiple transformers (Boteler, 2001; Bolduc, 2002). Simultaneously power loss was also reported in Sweden (Allen et al., 1989). More recent examples are the Halloween storm in 2003 which had strong Pc5 pulsations (Heyns et al., 2021) known to cause damage to power grids at mid-latitudes (Gaunt & Coetzee, 2007) and the St Patrick's day storm in 2015 which not only recorded GICs in the high-latitude regions but also at two equatorial stations (Carter et al., 2016). During the May storm of 2024 GICs of 30–40 A were recorded in the subauroral region (Hajra et al., 2024; Lawrence et al., 2025).

© 2026. The Author(s).
This is an open access article under the terms of the Creative Commons Attribution License, which permits use, distribution and reproduction in any medium, provided the original work is properly cited.

15427390, 2026, 6, Downloaded from https://agupubs.onlinelibrary.wiley.com/doi/10.1029/2026SW004959 by British Geological Survey, Wiley Online Library on [31/07/2026]. See the Terms and Conditions (https://onlinelibrary.wiley.com/terms-and-conditions) on Wiley Online Library for rules of use; OA articles are governed by the applicable Creative Commons License

Studies that use GIC measurements are usually focused on local impact across a region. The expense and technical expertise required to have instruments specifically fitted to high voltage AC transformers on the power grid and other infrastructure to measure GICs limits the number of measurements (Marshall et al., 2012; Watari et al., 2021). Watari et al. (2021) used instruments fitted to three Japanese substations and Hübert et al. (2024) used indirect measurements at 12 UK power grid sites. Though New Zealand has measurements from over 50 transformers (Rodger et al., 2017). Instead many studies focus on the rapid change in the magnetic field that can be used as a proxy for GIC, these are called geomagnetic disturbances (GMDs) or dB/dt fluctuations (Boteler et al., 1998; Rogers et al., 2021; Schillings et al., 2022; Viljanen, 1997). In this study we used GMDs to describe real events and spikes to refer to erroneous data. 1-minute cadence ground magnetometer data has been available in digital format since the early 1980s and has been the basis of many studies showing the frequency and intensity of GMDs (Freeman et al., 2019; Milan et al., 2023; Orr et al., 2021; Schillings et al., 2022).

Recently it has been suggested that using higher cadence magnetometer data could provide more accurate measurements of dB/dt to fully understand the effect of short lived GMDs as some GMD events will fall between adjacent minute cadence bins and be smoothed out leading to a smaller dB/dt (Schillings et al., 2022; Smith et al., 2025). There are three timescales on which extreme variations of dB/dt have been observed, where extreme is over 300 nT/min (5 nT/s) (Molinski et al., 2000). These timescales are hours, several minutes and tens of seconds which are related to magnetic storms, substorm activities and sudden commencements respectively (Kataoka & Ngwira, 2016). Also, GMDs may have a duration less than 60 s, which means a 60 s weighted average will reduce their amplitude. Therefore 1-s data could play an important part in the understanding the different drivers of the GMDs. Some previous studies have investigated this such as Grawe et al. (2018); Trichtchenko (2021) and Hartinger et al. (2023) who showed the importance of the higher cadence data during particular geomagnetic storms.

In this study we use all the data, not just storm time data, from SuperMAG ground magnetometer stations with 1-s measurement cadence between 2010 and 2020 we investigate the difference in the magnitude and number of GMDs when measured in the 1-s, 10-s median and 1 min data in order to see how the cadence of the data affects the number and amplitude, of GMDs observed at different magnetic local times and magnetic latitudes.

2. Data

We use data from SuperMAG which is a global collaboration providing data from ground based magnetometers. The SuperMAG data have been pre-processed and converted to the NEZ coordinate system and baseline-removed using the SuperMAG analysis technique (Gjerloev, 2012). N-direction is local magnetic north, E-direction is local magnetic east and *Z*-direction is vertically downwards. We consider each direction separately. The SuperMAG stations either provide data at 1-minute, or 1-s cadence or both. There are fewer stations with 1-s data than 1-minute data. 1 minute data have been available since the 1980s but 1-s data have only been available more recently, since the 2000s (Clarke et al., 2013; Macmillan & Olsen, 2013). We only use stations that provide both 1-s cadence data and 1-minute cadence data between 2010 and 2020 which amounts to 183 stations. We point out that there is a difference between absolute observatories and variometer stations. Variometer stations are not as well calibrated or maintained but there are many more of them compared to the observatories therefore we use both in this study. In this study we keep the component direction of the magnetometers separate using dB_i/dt to indicate that the respective GMD is any of the three components.

From these stations we use the 1-minute SuperMAG data product and compare with the 1-s SuperMAG data product and median filtered 10-s data. 10-s data are used as an intermediary product to remove erroneous and noisy readings from the 1-s data but still provide a higher cadence than the 1 min data. Each 10-s value is calculated taking the median value of the data for each 10-s window. The median is used instead of the mean to reduce the effect of single erroneous data points. A total of 183 stations are used in this study although these are not all available concurrently or continuously though the time period investigated. Some stations are also removed from the data set for particular years where there are unreliable data with GMDs being almost constantly recorded. This is determined using 30 min MLT bins. If over 95% of the bins have detections of GMDs in the 1-s data, where the GMD is greater than 5 nT/s, then the stations are removed from the study. This threshold was chosen in order to only remove stations where GMDs are almost constantly recorded at all magnetic local times due to instrumental or electronic effects rather than real GMDs. Table 1 shows the number of stations used each year and at which magnetic latitude range they are situated. The number in brackets is the total number of stations available.

Table 1
Number of Magnetometer Stations Used in This Study as Described in the Text

Year	Number of stationS	High MLat	Mid MLat	Low MLat
2010	100	4	46	50
2011	94	4	45	45
2012	97	2	46	49
2013	101	6	44	51
2014	103	6	46	51
2015	73	4	34	35
2016	75	5	44	26
2017	67	5	44	18
2018	62	6	38	18
2019	54	8	33	13
2020	49	3	36	10

Note. The last three columns show the number of magnetometer stations at different magnetic latitudes. High is greater than 70°, low is less than 50° and mid is between 50 and 70°.

The number of stations at the different latitudes changes over the years as new stations become operational or existing ones are decommissioned.

In order to compare dB/dt values from the different cadence data it is assumed that the GMDs occur evenly over the timestep and hence is calculated using the difference between consecutive data points and dividing by the time step, in seconds, between them.

We also use data from the THEMIS ASI (Time History of Events and Macroscale Interactions During Substorms all Sky imager). The THEMIS array covers a large area of the auroral oval over the North American continent with a temporal cadence of 3 s and operates continuously though northern winter between 00:00-15:00 UT which is approximately 17-07 MLT at each individual station (Donovan et al., 2006). We use stations at Athabasca, The Pas and Gillam in Canada and Kiana in Alaska with station code atha, tpas, gill and kian respectively. These stations are colocated with the SuperMAG stations with codes T36, T33, GIM, T41 respectively.

Finally we use magnetic indices AU, AL, SymH and SMR from OMNI data set (King & Papitashvili, 2005).

3. Results

Figure 1 shows an example of a GMD recorded at A08, a low latitude station in Davao, Philippines on the 17-Mar-2015 between 04:00-05:00 UT in the three magnetic components. The black lines show the 1 min data, the red line is the 10-s data and the blue line is the 1-s data. The columns are the directions N, E and Z respectively. The first row is the magnetic field data. The second row is the rate of change of the magnetic field in the component directions(dB/dt). This is found using the difference between consecutive data points and dividing by the time step, in seconds, between them. The

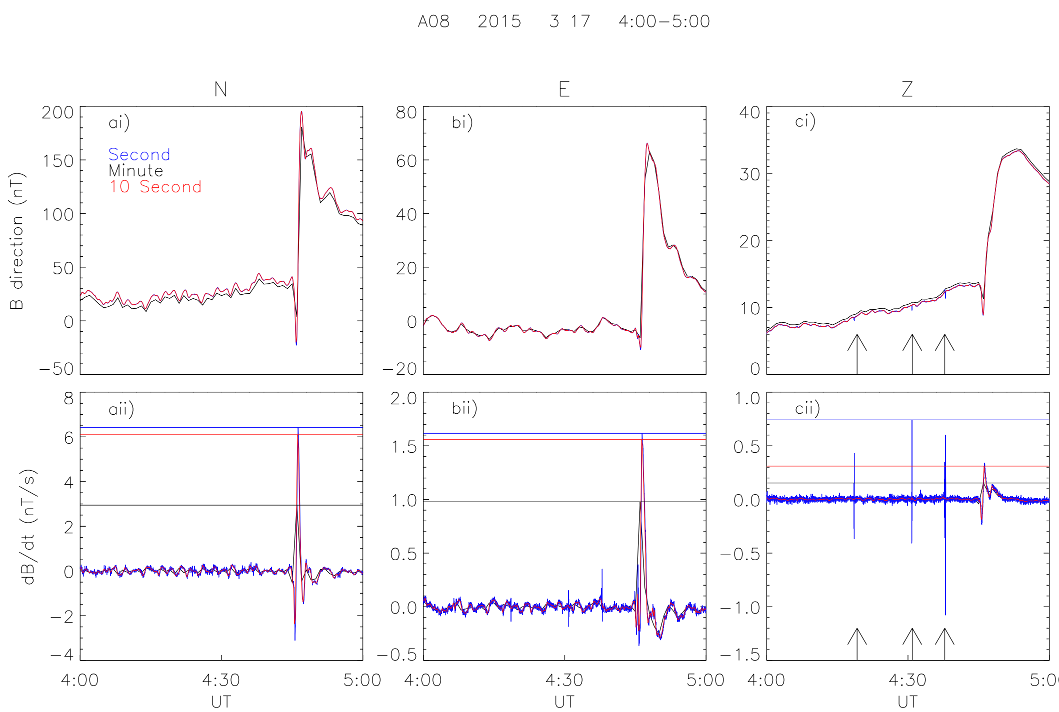

Figure 1. Example 1 2015/03/17 4:00-5:00 UT data from A08 station, Davao, Philippines (Low latitude station). First row (i) is magnetic field data in N, E and *Z* direction. Second row (ii) is dB/dt for N, E and *Z* direction. Black line is 1 min data. Blue line is 1-s data and red line is down sampled 10-s data. The horizontal line in the dB/dt panels are the maximum positive dB/dt for each data set in the hour. Arrows indicate artefacts in the 1-s data.

15427390, 2026, 6, Downloaded from https://agupubs.onlinelibrary.wiley.com/doi/10.1029/2026SW004959 by British Geological Survey, Wiley Online Library on [31/07/2026]. See the Terms and Conditions (https://onlinelibrary.wiley.com/terms-and-conditions) on Wiley Online Library for rules of use; OA articles are governed by the applicable Creative Commons License

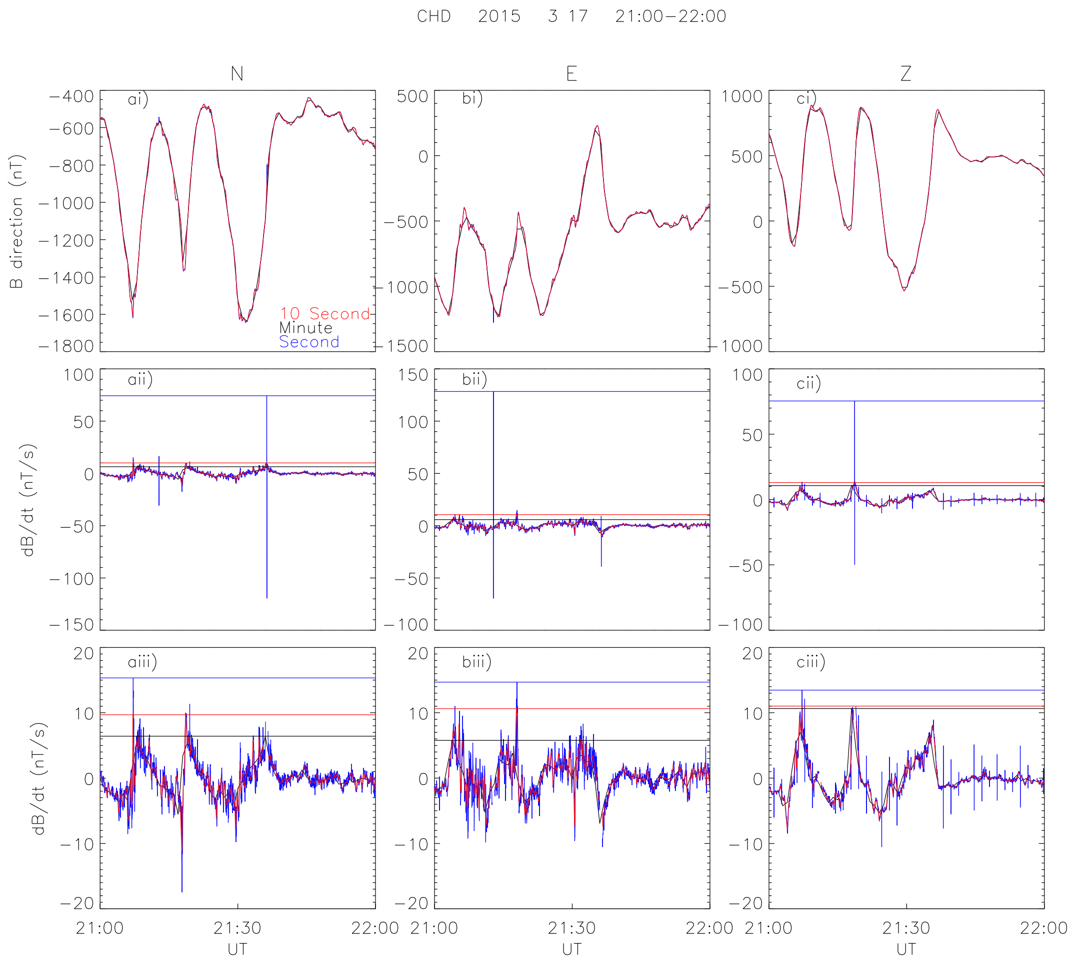

Figure 2. Example 2 2015/03/17 21:00-22:00 UT data from CHD station, Chokurdakh, Russia (Mid Latitude station). Rows one and two are the same format at Figure 1. Row three is the dB_i/dt calculated from corrected magnetic field data as described in the text.

horizontal lines show the maximum positive dB/dt during the hour of data shown for each data set for ease of comparison. This is an example of a storm sudden commencement (SSC) which is typically the onset of a geomagnetic storms.

All three data sets lie close to each other for the magnetic field measurement. The difference comes when looking at the dB_i/dt. The maximum dB_i/dt for this event occurs in the N direction and is larger for the 1-s data (6.5 nT/s) than the 1 min data (3 nT/s). These respective maximums occur at approximately the same time and are related to the same feature and magnetic change. Additionally, there are examples of maximums in the 1-s data that are not replicated in the 1-minute data in Figure 1cii, indicated by the arrows. These are likely artefacts in the 1-s data, in these cases the resulting dB_Z/dt is small and do not interfere with studies of GMDs however this is not always the case.

A second example shown in Figure 2 clearly highlights this issue with the 1-s data when looking for the maximum dB_i/dt. It shows some quasi-periodic spikes that suggest there is some local contamination either from some electrical equipment on site or perhaps a local train system. There is a small deviation from the expected values just before 21:15 in the E direction (Figure 2bi). This leads to a very large dB_E/dt (Figures 2bii 130 nT/s) but this is not believed to be real due to the local contamination. 1-s geomagnetic data are often contaminated by instrumental or electronic effects. In particular, a slight voltage drop in the instrument can cause a difference in measurement of the full field value. There can also be digitisation errors, sampling or timing errors. Where there are effects in two or three components, it is likely an instrumentation problem. Where the issue affects only one value that is more likely to be a package transmission error between the instrument and the logging machine when

15427390, 2026, 6, Downloaded from https://agupubs.onlinelibrary.wiley.com/doi/10.1029/2026SW004959 by British Geological Survey, Wiley Online Library on [31/07/2026]. See the Terms and Conditions (https://onlinelibrary.wiley.com/terms-and-conditions) on Wiley Online Library for rules of use; OA articles are governed by the applicable Creative Commons License

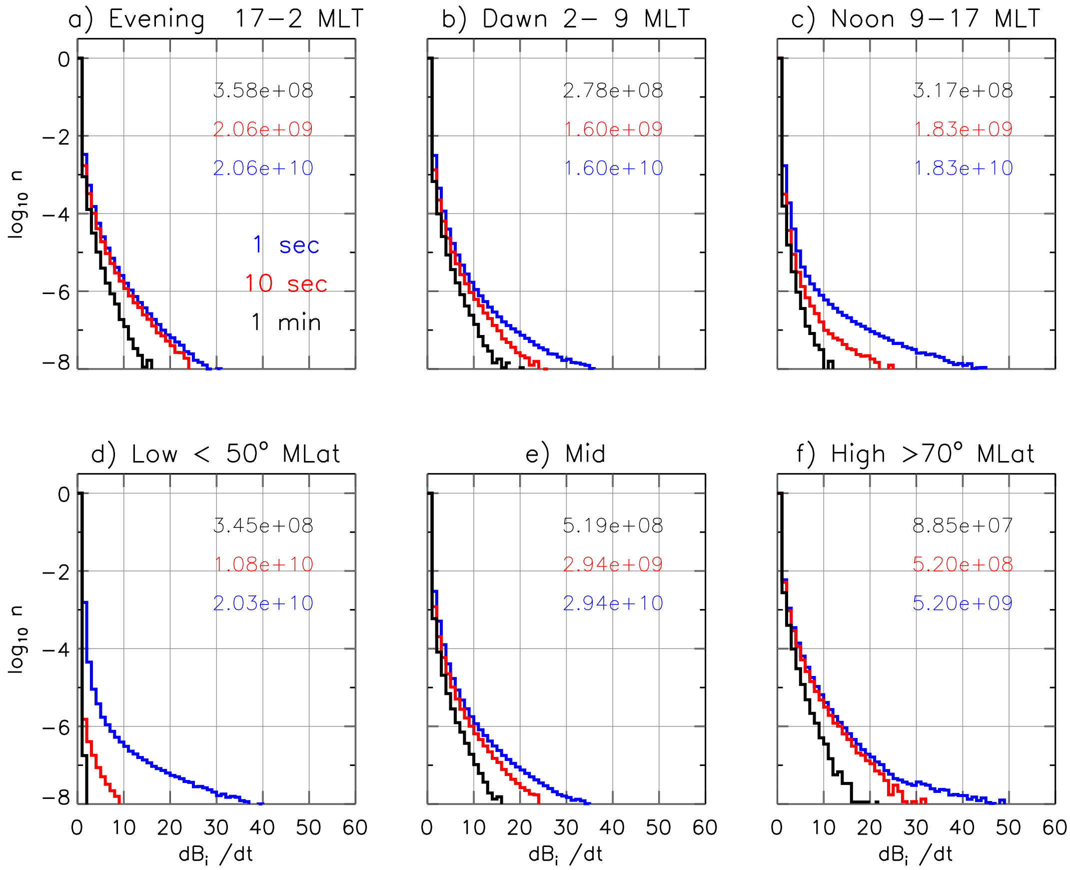

Figure 3. Histogram of the absolute magnitude of GMDs between 2010 and 2020 in 1 nT/s bins on a log scale, where n is the relative number of GMDs calculated from the number of GMD in the 1 nT/s bin divided by the total number of GMD for that cadence data and magnetic local time (MLT) or MLat group. 1-s data are in blue, 10-s in red and 1-minute data in black. The numbers in the top right of each panel is the number of GMDs included in the line of the corresponding color. (a) Evening GMDs between 17 and 2 MLT (b) dawn GMDs between 2 and 9 MLT (c) noon GMDs between 9 and 17 MLT (d) low latitude stations less than 50° magnetic latitude (e) medium latitude stations between 50 and 70° magnetic latitude and (f) high latitude stations greater than 70° magnetic latitude.

data are sent along the connecting cables to be recorded. The 1-s data have far more artefacts than the 1-min data due to the fact that the 1-min data is typically re-sampled from the 1-s data. SuperMAG re-samples the data using median filtering. This process, in contrast to averaging, is insensitive to spikes. Additionally, SuperMAG has an automated spike removal routing (absolutely necessary but it only removes clear and obvious spikes) and erroneous data manually identified in the 1-min data set are removed from the 1-sec data set. Despite these efforts there remain some artefacts in the 1-sec data set.

In order to perform statistics on the whole data set it is important first to remove any unreliable data from the 1-s data. For the 1-s data, data points within 15 s of a data gap are removed, along with data either side of an unreliable spike. 15 s is chosen to sufficiently remove erroneous reading around data gaps but not to remove too much data. A data gap is consecutive missing data points above 5 missing points. A spike is considered unreliable if the absolute dB_i/dt value is greater than 5 nT/s and the neighboring data point is also greater than 5 nT/s but in the opposite direction. 5 nT/s is chosen as a threshold to be comparable with previous studies (Fleetham et al., 2024; Milan et al., 2023). In this case, data are removed from the 30 s period centered on the bad data point, this removes 15 s on either side of the bad data as with the data gaps. All values of dB_i/dt above 500 nT/s are also removed. Figure 2iii show the corrected dB_i/dt for the event which is then used for the statistics. The 10-s median filtering removes the unreliable data from the from the 10-s data due to the re-sampling in the same way as the 1-min data.

Figure 3 shows the histograms of the absolute magnitude of GMDs between 2010 and 2020 in 1 nT/s bins on a log scale. The data are separated into the MLT in Figures 3a–3c). Evening is between 17 and 2 MLT, dawn is between

15427390, 2026, 6, Downloaded from https://agupubs.onlinelibrary.wiley.com/doi/10.1029/2026SW004959 by British Geological Survey, Wiley Online Library on [31/07/2026]. See the Terms and Conditions (https://onlinelibrary.wiley.com/terms-and-conditions) on Wiley Online Library for rules of use; OA articles are governed by the applicable Creative Commons License

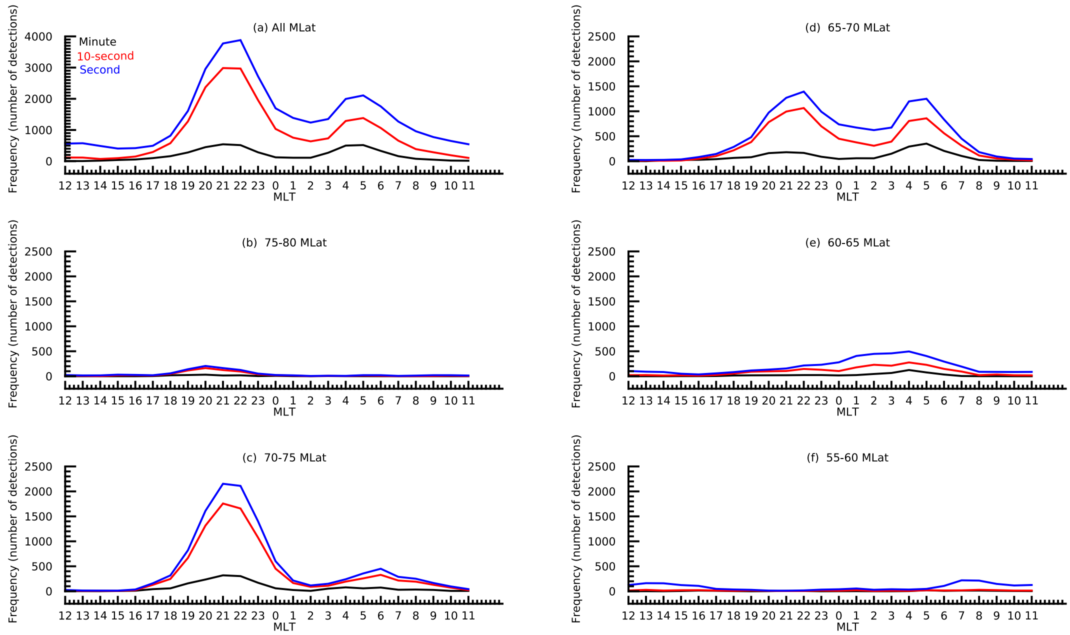

Figure 4. Histograms of the number of GMDs by magnetic local time in 1 hr bins. Black minute data, blue 10-s and red 1-s. (a) Contains all data. (b–f) Data from different MLat regions in 5° bins from 55 to 80° MLat.

2 and 9 MLT and noon is between 9 and 17 MLT. These are chosen to be the same as those used by Milan et al. (2023) and Bower et al. (2024) and loosely cover local times related to substorm GMDs, dawn sector GMDs, and other local times. The 1 min data (black) record lower dB_i/dt and the 1-s data (blue) record the highest dB_i/dt. The 10-s data (red) lie in between the two. The largest difference between the 1-minute and the 1-s data is for the noon GMDs with a difference in the maximum GMD of around 30 nT/s. This is also the largest difference between the 10-s data and the 1-s data with a difference in the maximum GMD of around 20 nT/s. The smallest difference between the data set is for the evening GMDs with the maximum GMD of around 15 nT/s, 25 nT/s and 30 nT/s for the 1-min, 10-s and 1-s data respectively.

Figures 3d–3f show the histograms with the data separated by the magnetic latitude (MLat) of the stations. Figure 3d is the low MLat stations below 50° magnetic latitude (77 stations). Figure 3e is the mid latitude stations between 50 and 70° magnetic latitude (78 stations). Figure 3f is high latitude stations above 70° magnetic latitude (12 stations). The number of stations is the number of unique stations used, they are not all available every year. The boundaries were chosen as it has previously been shown there is an increase in the magnitude of dB/dt above 50° magnetic latitude (Carter et al., 2016; Ngwira et al., 2013; Pulkkinen et al., 2012). Therefore we chose low latitude stations to be below this. The high stations were chosen to be above 70° MLat as there is another boundary in the median probability of magnetic activity at this point (Hughes et al., 2022; Viljanen & Tanskanen, 2013) (Table 1 shows the number of stations per year at each MLat category). From Figures 3d–3f) we can see that at low latitude there are not many GMD detected in the minute data but almost two orders of magnitude more detected in the 1-s and 10-s data. For the low latitude the number of GMDs are of the same order of magnitude for the 10-s data and the 1-s data but the maximum GMD is considerable higher for the 1-s data at around 40 nT/s compared to 10 nT/s for the 10-s data. The maximum GMD in each data set is in the high latitude region.

The number of GMDs detected in each MLT sector is compared to determine if the higher cadence is more important for particular formation mechanisms of GMDs. Figure 4 shows histograms of the number of GMDs in 1 hr MLT bins. Again, the black line is the minute data, the red 10-s data and the blue 1-s data. In order to display on the same scale the 1-s and 10-s values have been divided by 60 and 6 respectively. Panel (a) contains all the data whereas panels (b-f) are the GMDs plotted in different 5° MLat bins. From Figure 4a it can be seen that more GMDs are detected evening for the higher cadence data where the minute data has smaller comparable height peaks at dawn and evening.

15427390, 2026, 6, Downloaded from https://agupubs.onlinelibrary.wiley.com/doi/10.1029/2026SW004959 by British Geological Survey, Wiley Online Library on [31/07/2026]. See the Terms and Conditions (https://onlinelibrary.wiley.com/terms-and-conditions) on Wiley Online Library for rules of use; OA articles are governed by the applicable Creative Commons License

15427390, 2026, 6, Downloaded from https://agupubs.onlinelibrary.wiley.com/doi/10.1029/2026SW004959 by British Geological Survey, Wiley Online Library on [31/07/2026]. See the Terms and Conditions (https://onlinelibrary.wiley.com/terms-and-conditions) on Wiley Online Library for rules of use; OA articles are governed by the applicable Creative Commons License

From Figure 4a it can be seen that for the higher cadence data more GMDs are detected evening, peaking at 22 MLT, than at dawn which peaks at 5 MLT. For the Minute data the number of GMDs at evening and dawn are more comparable. It can be seen by comparing Figures 4b–4f that the evening GMDs occur at higher MLat than the dawn GMDs which occur primarily between 60 and 70 MLat.

For a direct comparison between the GMD values measured we investigated the magnitude of the GMDs in the minute data and compared it to the maximum magnitude GMD in the second data for the corresponding minute (Figures 5a–5f) and to the maximum magnitude GMD in the 10-s data for the corresponding minute (Figures 5g–5l). The corresponding minute is determined using the 30 s before and 30 s after the minute mark. Figure 5 includes data from every minute between 2010 and 2020. The data are separated by MLT (a–c) (g–i) and MLat (d–f) (j–l). Each plot has a butterfly type shape. However, it can be seen that the GMDs in the second data are usually higher than the minute data for the same time period. The low latitudes distribution has a smaller range of GMD magnitudes with a lower frequency GMDs above 7 nT/s in the second data than the other latitude ranges. The noon GMDs also have a smaller magnitude GMD in the minute data with the absolute magnitude of the GMD rarely exceeding 4 nT/s compared to the dawn and evening MLT sectors which regularly reach higher values up to 6 nT/s. This can also be seen in the second data with more GMDs with an absolute magnitude of above 10 nT/s for the dawn and evening MLT sectors than the noon sector. It can also be seen that for some events the direction of the GMD is opposite in the minute data compared to the second data. This is due to the variable nature of the second data and is discussed further below.

4. Discussion

Using stations that provide SuperMAG 1-s cadence data we have investigated the difference in the number and magnitude of GMDs recorded between the 1-s data and the minute cadence data as well as a down sampled 10-s data derived from the 1-s values. As expected the 1-s data consistently records higher GMDs than either the minute or the 10-s data (Figure 3).

We divide the data into three latitude bins, high, medium and low magnetic latitude. From Figure 3 it is clear that the magnitude of GMDs recorded at the low latitude stations are different. The number of minute data with larger GMDs declines rapidly so that there are no extreme GMDs, greater than 5 nT/s, detected in this time period from these stations. However, there is clear evidence of extreme GMDs in the 1-s and 10-s data. This shows the importance of the second data to detect the rapid GMDs at low latitudes.

Separating the data by MLT, a small difference can be seen in the maximum magnitudes. The data are split using the same MLT sectors as Milan et al. (2023); Bower et al. (2024) this is that dawn is 2–9 MLT, noon is 9–17 MLT and evening is 17-2 MLT. From Figures 3a–3c it can be seen that the maximum magnitude in the second data is lower for the evening sectors than the other two; however for the minute data the maximum magnitude is lowest in the noon. This suggests that the higher cadence data is especially important for investigating the noon GMDs as this is when the largest difference between the minute and second data occurs for high magnitude GMDs.

The intensity plots in Figure 5 show the majority of the data lies between the diagonal line of x equals y and the x-axis in the region where the dB_i/dt is higher in the 1-s data than the minute data. Some events are seen to have GMDs in the opposite direction when comparing the minute and maximum value in the second data for the corresponding minute. Figure 6a shows an example with an hour of data centered on a GMD event with opposite signs. The top panels show the N direction magnetic field data. The middle panels are the dB_N/dt data and the bottom panels are the dB_N/dt with the maximum value of the second data for each minute. From Figure 6a it is clear to see the variable nature of the 1-s data and how the minute data provide a less accurate description of the magnetic field in both magnitude and direction when compared to the 1-s and 10-s data.

There is also a band of higher intensity around the x-axis (Figure 5) where the minute data is close to zero, this due to rapid dB_i/dt in the 1-s data, that are short lived occurring over few seconds, the majority of these are not believed to be real and are artefacts in the 1-s data that cannot easily be removed (Figure 6b). Using 10-s data instead removes the band along the x-axis (Figures 5g–5i). This band is likely the reason for the number of high magnitude noon GMD in the second data set being slightly above the evening GMD line in Figure 3c.

The slight vertical band around the y-axis where the second data are between 5 nT/s and −5 nT/s, most prominently seen in mid magnetic latitude data (Figure 5e), is linked to the removal of unreliable dB_i/dt in the second data. All dB_i/dt spikes are checked to see if they are unreliable only if they are over 5 nT/s; there is potential that

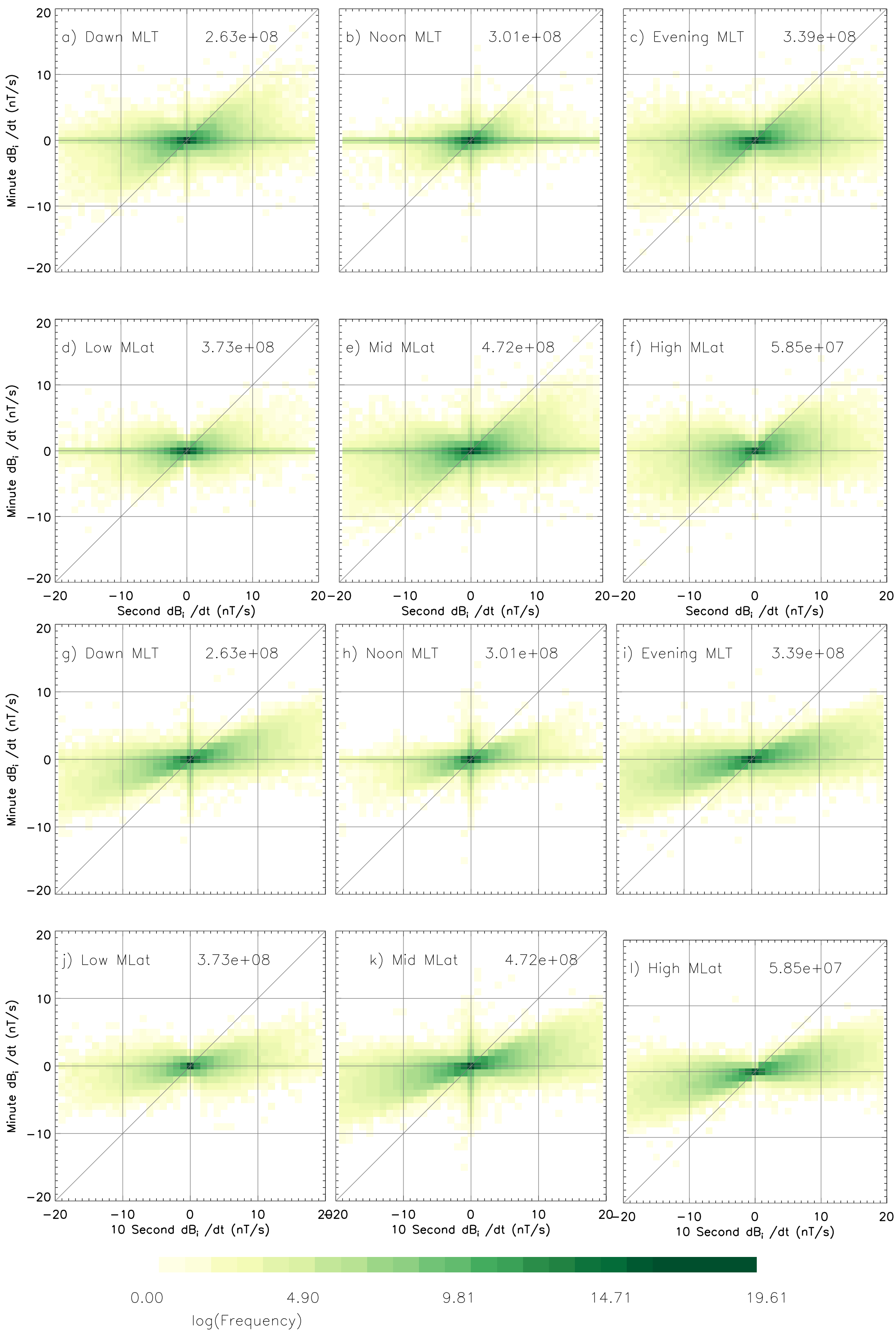

Figure 5. Intensity plots of the magnitude of the dB$_i$/dt in the minute data compared with the maximum magnitude for the corresponding minute of the (a–f) 1-s data (g–i) 10-s data. Panels arranged by magnetic local time and MLat. The diagonal line of equivalence is added to as a guide.

15427390, 2026, 6, Downloaded from https://agupubs.onlinelibrary.wiley.com/doi/10.1029/2026SW004959 by British Geological Survey, Wiley Online Library on [31/07/2026]. See the Terms and Conditions (https://onlinelibrary.wiley.com/terms-and-conditions) on Wiley Online Library for rules of use; OA articles are governed by the applicable Creative Commons License

15427390, 2026, 6, Downloaded from https://agupubs.onlinelibrary.wiley.com/doi/10.1029/2026SW004959 by British Geological Survey, Wiley Online Library on [31/07/2026]. See the Terms and Conditions (https://onlinelibrary.wiley.com/terms-and-conditions) on Wiley Online Library for rules of use; OA articles are governed by the applicable Creative Commons License

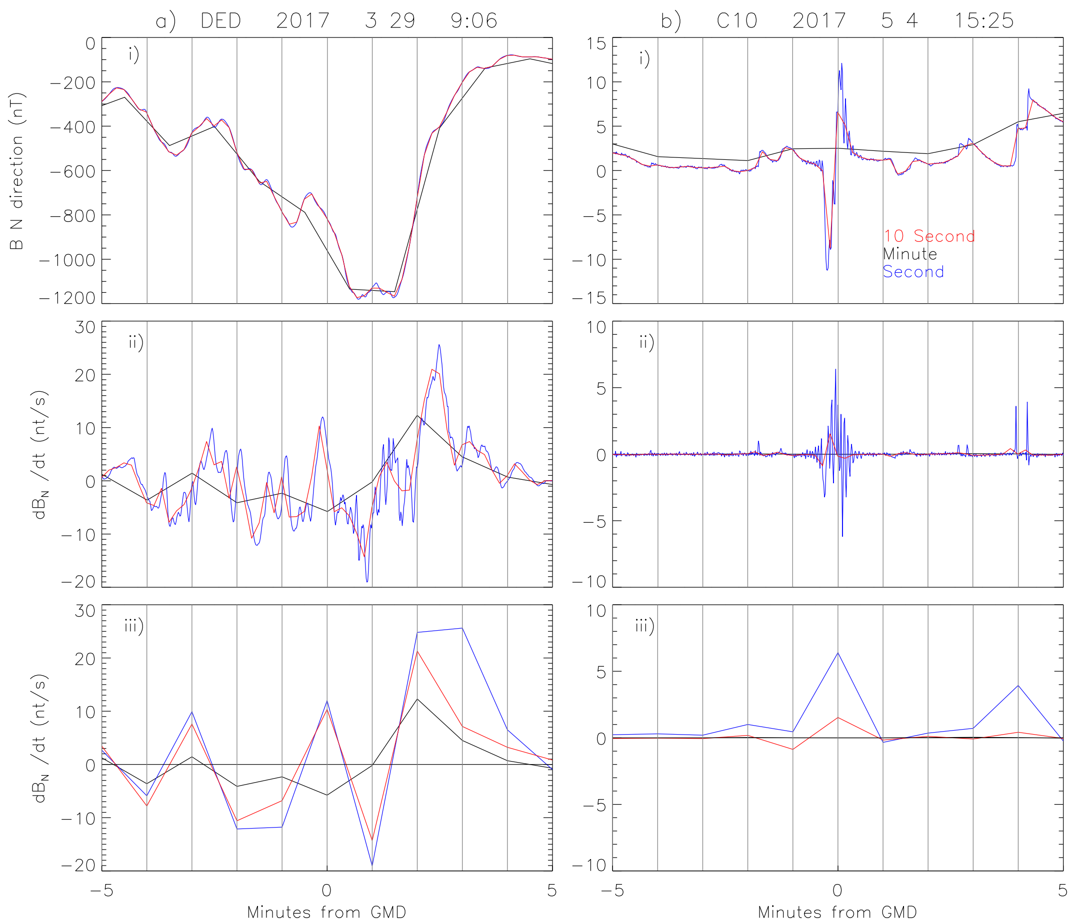

Figure 6. (a) Example GMD with maximum magnitude in opposite direction in minute and 1-s data. 2017/03/28 at 9:06 UT data from DED station, Deadhorse, Alaska. (b) Example artefacts in the 1-s data. 2017/05/03 at 15:25 UT data from C10 station, Polson, Montana. (i) N direction magnetic field data. (ii) Rate of change of the magnetic field. (iii) Rate of change of magnetic field using maximum value in each minute. Black line is minute data, red is 10-s data and blue is 1-s data.

GMDs have been removed leaving only values less than 5 nT/s in the corresponding minute. This suggests that the mid latitude data are the most variable as they have the clearest band below 5 nT/s.

Of most interest are the large GMDs as they are the ones most likely to damage infrastructure. Although many factors affect whether a GMD will cause a harmful GIC (Grawe et al., 2018; Pulkkinen et al., 2008) and these have been classified into four groups for power grid vulnerability including GMD parameters as one factor (Sokolova et al., 2018). Molinski et al. (2000) describe severe events as having a 300 nT change in the magnetic field in 1 min. Therefore using a 5 nT/s threshold, as has previously been used by Milan et al. (2023) and Fleetham et al. (2024) the example shown in Figure 1i would be missed in the minute data.

4.1. Impact on GMD Populations

Finally we discuss the impact of the higher cadence data on the different GMD populations. Three populations of large GMDs are known to occur, evening, dawn and a smaller pre-noon population (Fleetham et al., 2024; Milan et al., 2023; Schillings et al., 2022). The evening population has previously been shown to be related to substorm activity due to the electrojets and the formation of the substorm current wedge (Juusola et al., 2015; Milan et al., 2023; Schillings et al., 2022; Weigel et al., 2002). We can see from Figure 4 that the evening population is the dominant population for the 1-s and 10-s data but for the 1-min data the peaks are comparable in the evening sector and the dawn sector. This can be explained by the rapid decrease in the magnetic field due to substorm onset where, as shown in Figure 7a, the magnetic gradient is smoothed in the minute data and therefore missed. Figure 4 also shows that the evening population of GMDs occurs between 65 and 75 MLat which is similar to the location

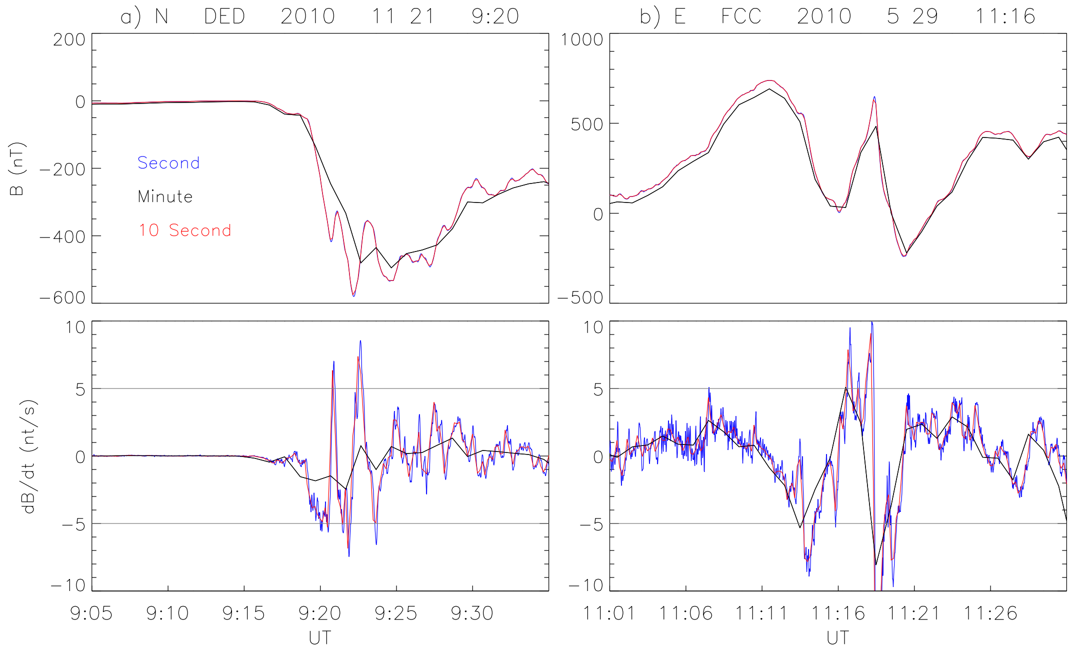

Figure 7. (a) Example of a substorm related GMD in 1-s and 10-s data not detected in 1-m. 2010/11/21 at 9:20 UT data from DED station, Deadhorse, Alaska located at 21.5 magnetic local time (MLT). (b) Example of a dawn GMD detected in all three data sets. 2010/5/29 at 11:16 UT data from FCC station, Fort Churchill, Canada located at 4 MLT.

of substorm onset (65–70) (Liou et al., 2001; Tanskanen et al., 2002) and supports that these GMDs are substorm related and the need for the higher cadence data to capture the full change in the magnetic field related to substorms.

The dawn population on the other hand is believed to be related to omega bands (Juusola et al., 2015; Milan et al., 2024; Schillings et al., 2022) and the formation of a dawn side current wedge (Bower et al., 2025; Ohtani et al., 2018; Sorathia et al., 2022). This leads to more wave-like signatures in the magnetometer data from the related quasi-periodic pulsations with 5–10 min period (Viljanen et al., 2001; Vokhmyanin et al., 2021) therefore less smoothing occurs for the dawn population GMDs and they are more similarly represented in all three data sets (Figure 7b), although with higher magnitudes still recorded in the higher cadence data. We show that the dawn population also primarily occurs at lower MLat than the evening, GMDs between 60 and 70 MLat (Figure 4). This is in agreement with the peak location of omega bands at 64 MLat as found by Partamies et al. (2017).

The evening and dawn populations have been considered as two distinct populations (EPRI, 2020; Milan et al., 2023; Schillings et al., 2022) however Milan et al. (2023) noted the curious relative lack of GMDs in the 00 to 03 MLT sector compared to the evening and dawn sectors despite frequent aurora activity in the 00–03 MLT sector. From Figure 4a we can see that the number of GMDs in the 2 MLT sector compared to the 5 MLT sector is higher for the second data with a ratio of 0.59 compared to 0.21 for the minute data. This suggests that the 0–3 MLT sector has more rapid GMDs that are missed in the minute data. One possibility for the origin of these rapid GMDs is pulsating aurora. Pulsating aurora are rapidly varying patches of diffuse aurora that brighten and dim on time scales of 1–40 s (Johnstone, 1978; Lessard, 2012; Royrvik & Davis, 1977; Yang et al., 2017). They are predominately seen to occur during the expansion and recovery phase of substorms and after magnetic midnight (Jones et al., 2011; Zou et al., 2022). Zou et al. (2022) showed an example of geomagnetic disturbances co-located with pulsating aurora that occurred on the 1 November 2016 during a storm recovery phase and a substorm recovery phase. The pulsating aurora occurred predominately between 64 and 67 MLat over KIAN ASI which was located in the 02–03 MLT sector at this time. They noted that the large dB/dt seen had characteristic high frequency fluctuating pattern that could only be detected in high cadence magnetometers. This supports the idea that GMDs relating to pulsating aurora could filling the 00–03 MLT which appears as a gap in the minute data but not in the second and 10-s data.

15427390, 2026, 6, Downloaded from https://agupubs.onlinelibrary.wiley.com/doi/10.1029/2026SW004959 by British Geological Survey, Wiley Online Library on [31/07/2026]. See the Terms and Conditions (https://onlinelibrary.wiley.com/terms-and-conditions) on Wiley Online Library for rules of use; OA articles are governed by the applicable Creative Commons License

Zou et al. (2022) also performed a statistical study on the type of aurora related to the GMDs in the different MLT sectors they focused only during geomagnetic storms (Dst < −50 nT) between 2015 and 2016. They showed post-midnight (1.5–4.5 MLT) to be dominated by pulsating aurora related GMDs followed by omega bands. Their midnight sector (22.5–1.5 MLT) also including many (23.4%) pulsating aurora related GMDs alongside a wide range of other types of aurora related GMDs.

A subset (18) of the magnetometers used in this study are aligned with THEMIS ASI. Figure 8 shows an event on the 5th April 2010 between 9 and 10 UT that has pulsating aurora-related GMDs in the 0–3 MLT sector. The top panels show north-south keograms and the magnetometer data from three colocated stations. Panel (g) show the OMNI AU and AL index and panel (h) shows the OMNI symH in black and the SMR local time indices (SMR06, SMR12, SMR18, SMR00) in green, yellow, red and blue respectively.

This event takes place during the main phase of a storm that eventually reached SMR of −85 nT at 14:20 on 2010/04/06. With a prolonged southward turning of the interplanetary magnetic field after 12:45 on 2010/04/05 leading to rapid variations in SMU and separation in the SMR-LT values, which are signatures of multiple intensification (Bower et al., 2025; Milan et al., 2021, 2024) and are accompanied by many dawn GMDs in the high cadence data (not shown). The initial period of the storm shown in Figure 8 coincides with the increase of plasma density and speed of the solar wind due to a coronal mass ejection arriving at Earth which cause the large decrease in SMU and SMR00.

The pulsating aurora are the vertical stripes in the ASC keograms (Grono & Donovan, 2020) seen clearest in panel 8(a), this station also shows the most variability in the 1-s data (Figure 8b) and the maximum GMD from the stations shown during this time period.

It is important to note that typical pulsating aurora does not account for all the GMDs in the 00–02 MLT sector, there are other types of rapidly varying aurora happing at the same time in the same sector making it difficult to determine which is causing the GMD (Figure 8e). Figure 9 shows an example from later on the same day as Figure 8 this time showing a minute of data with the full ASI image. Although not typical pulsating aurora there are rapid variations in the aurora that are missed at 1 min cadence, that can lead to GMD such as the intensification in the auroral brightness at 13:11:36 which occurs alongside a change in the magnetic field than leads to a GMDs greater than 5 nT/s.

A complete study of different types of pulsating aurora and their relation to GMDs is outside the scope of this work.

It is also important to note that the 1-s data are not always reliable even after they have been post-processed using the SuperMAG, as there are many large artefacts in the data. Figure 2 clearly highlights this problem with a small deviation from the expected values at around 21:15 in the E direction which leads to a very large dB_E/dt that is not believed to be real. The removal process of unreliable spikes corrects for this only if the spike does not persist over more than one data point. This may lead to the some of the artefacts in Figure 5 as described above such as the higher intensity along the *y*-axis. Therefore it is believed that the number of GMD in the 1-s data is an over-estimate of the true number of real GMDs. The 10-s data removes the majority of these issues therefore the 10-s data is more reliable than the 1-s data at detecting real GMDs that are missed in the minute data.

5. Conclusion

We have shown that SuperMAG 1-s cadence data consistently records higher GMDs than the minute cadence data for the same stations and that this difference is most apparent in the low latitude stations and in the noon MLT sector. 1-s data are therefore important in understanding the most rapid changes in the magnetic field that could lead to GIC. We have shown that higher cadence data are of more importance for the evening substorm related GMDs than the dawn population of GMDs due to how rapid the related changes in the magnetic field are. We also show that high cadence data are of importance for GMDs in the post-midnight sector with the 0–2 MLT sector having proportionally more GMDs detected in the higher cadence data. We suggest this could be due to the presence of pulsating aurora in this sector; however further work is needed.

Due to the variability of the 1-s data, the 10-s data are currently better for large statistical studies where it is not possible to confirm the validity of each individual GMD. For studies focusing on single storm events 1-s data are more valuable as more large GMDs will be detected. However although the GMDs will be more prevalent with

15427390, 2026, 6, Downloaded from https://agupubs.onlinelibrary.wiley.com/doi/10.1029/2026SW004959 by British Geological Survey, Wiley Online Library on [31/07/2026]. See the Terms and Conditions (https://onlinelibrary.wiley.com/terms-and-conditions) on Wiley Online Library for rules of use; OA articles are governed by the applicable Creative Commons License

15427390, 2026, 6, Downloaded from https://agupubs.onlinelibrary.wiley.com/doi/10.1029/2026SW004959 by British Geological Survey, Wiley Online Library on [31/07/2026]. See the Terms and Conditions (https://onlinelibrary.wiley.com/terms-and-conditions) on Wiley Online Library for rules of use; OA articles are governed by the applicable Creative Commons License

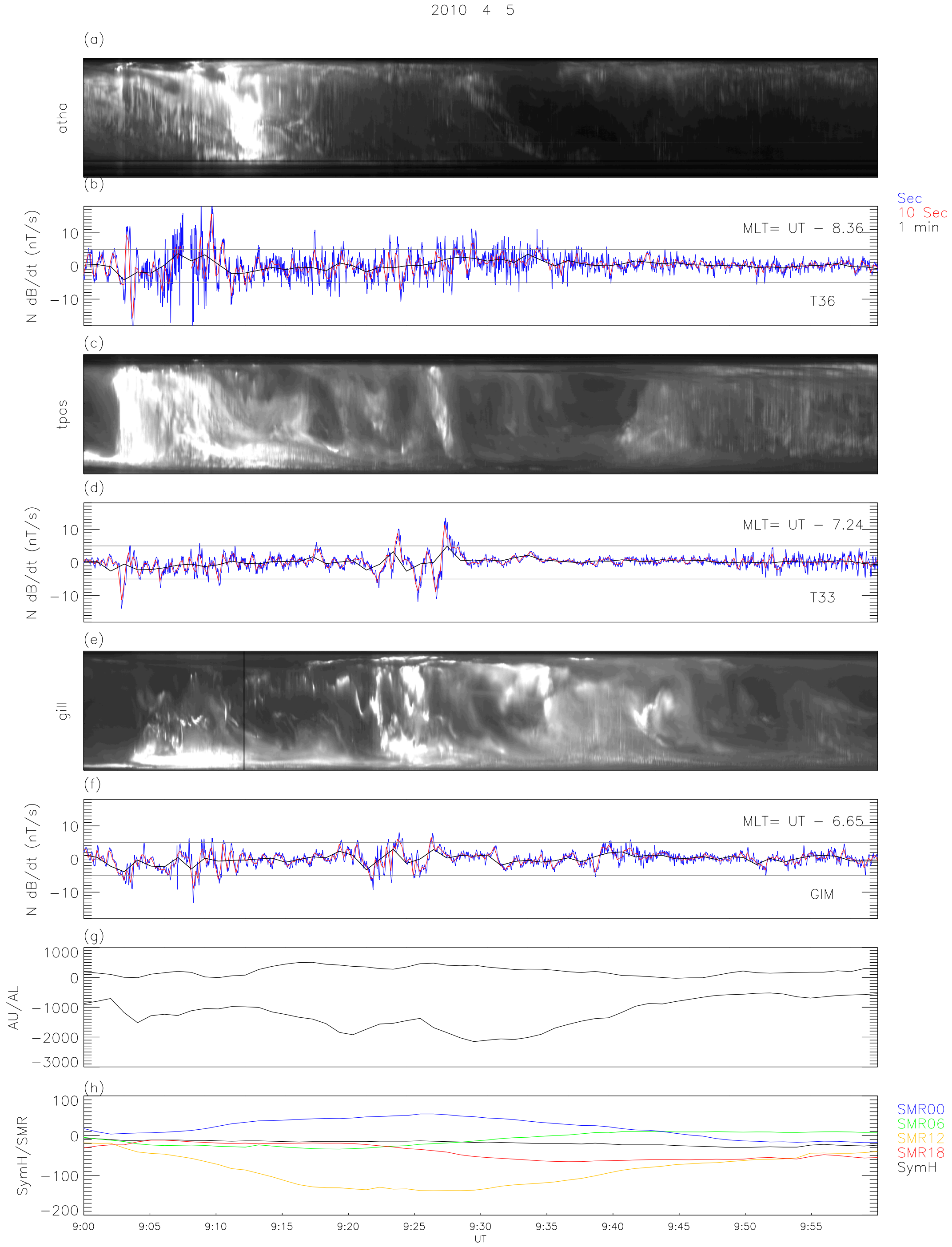

Figure 8. An example of pulsating aurora related GMDs on 2010/4/5. (a, c, and d) north-south keograms of THEMIS ASI data. (b, d, and e) colocated magnetometer data in the N direction. The black horizontal lines are the GMD threshold. (g) OMNI AU and AL index, (h) OMNI symH (black) and the SMR local time indices SMR06, SMR12, SMR18, SMR00 in green, yellow, red and blue respectively.

higher amplitudes, how much impact a GMD of less than a second would cause is likely to depend on the details of the industrial system the GMD occurs in. Rodger et al. (2017) found that 5 s resolution data was better at capturing the peak GIC in the Islington, New Zealand substation for their events. But this maybe different for other systems such as pipelines and railway networks.

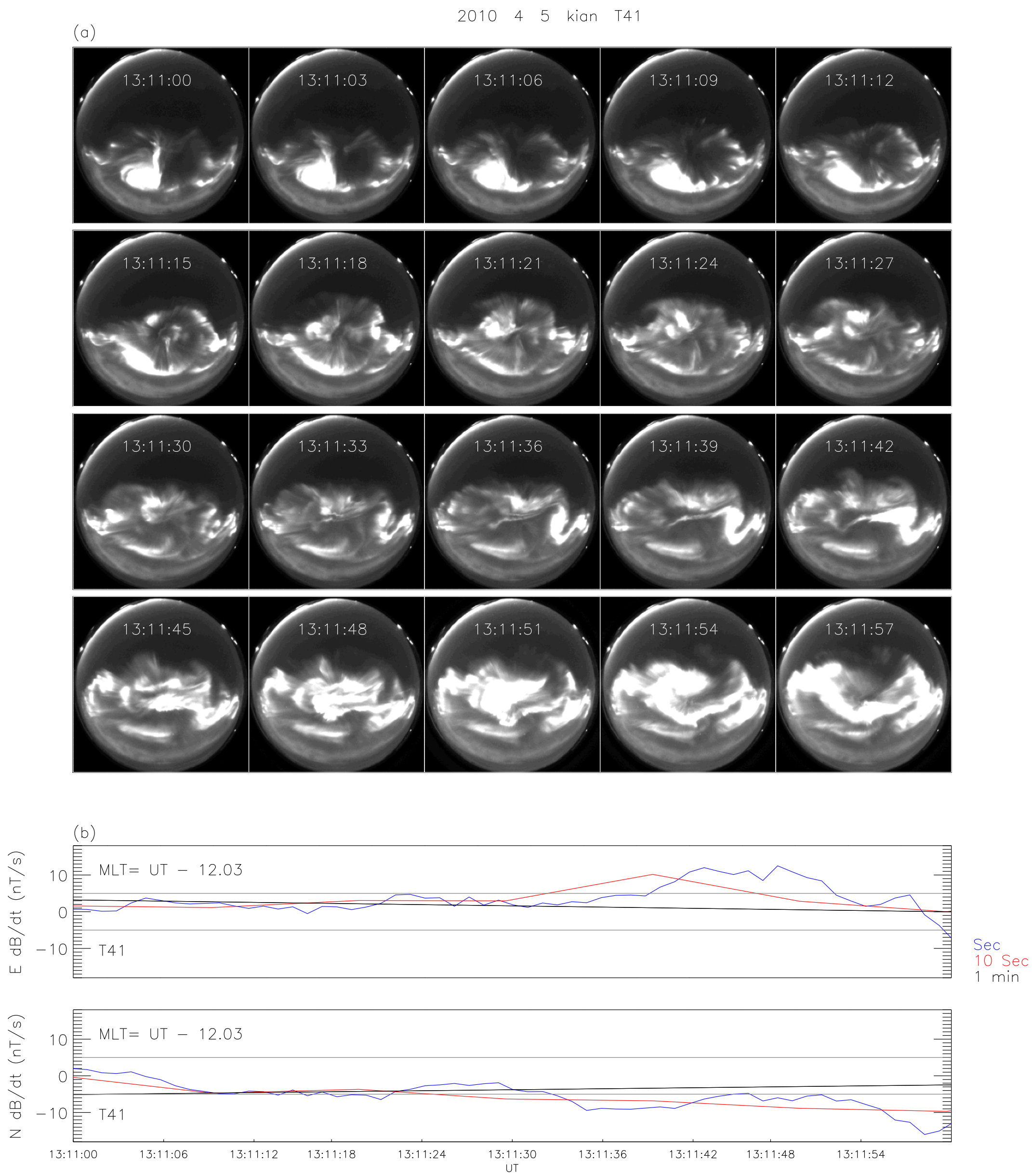

Figure 9. An example of rapidly varying aurora in ASI leading to GMDs in high cadence data on 2010/04/05 13:11 UT. (a) Kiana station ASI with north at the top.(b) dB/dt in the E direction from T41 which is colocated with Kiana ASI (c) dB/dt in the N direction. Black line is minute data, red is 10-s data and blue is 1-s data. The black horizontal lines are the GMD threshold.

Conflict of Interest

The authors declare no conflicts of interest relevant to this study.

Availability Statement

The 1-s cadence ("high fidelity") SuperMAG data were obtained through the SuperMAG portal at https://supermag.jhuapl.edu/mag/?fidelity=high (SuperMAG, 2023a). The 1-minute cadence ("low fidelity") SuperMAG data were obtained from NASA GSFC through the SuperMAG portal at https://supermag.jhuapl.edu/mag/?fidelity=low (SuperMAG, 2023b). The SuperMAG indices were obtained through the SuperMAG portal at https://superma

15427390, 2026, 6, Downloaded from https://agupubs.onlinelibrary.wiley.com/doi/10.1029/2026SW004959 by British Geological Survey, Wiley Online Library on [31/07/2026]. See the Terms and Conditions (https://onlinelibrary.wiley.com/terms-and-conditions) on Wiley Online Library for rules of use; OA articles are governed by the applicable Creative Commons License

15427390, 2026, 6, Downloaded from https://agupubs.onlinelibrary.wiley.com/doi/10.1029/2026SW004959 by British Geological Survey, Wiley Online Library on [31/07/2026]. See the Terms and Conditions (https://onlinelibrary.wiley.com/terms-and-conditions) on Wiley Online Library for rules of use; OA articles are governed by the applicable Creative Commons License

g.jhuapl.edu/indices (Newell & Gjerloev, 2012). The high cadence (1-min) OMNI data used in this study were obtained from the NASA Goddard Space Flight Center (GSFC) Space Physics Data Facility OMNIWeb portal at https://omniweb.gsfc.nasa.gov/form/om_filt_min.html (King & Papitashvili, 2005). The THEMIS ASI data (Donovan et al., 2006) used in this study was obtained from UCalgary Space Remote Sensing Open Data Platform at https://data.phys.ucalgary.ca/sort_by_project/THEMIS/asi/stream0.

Acknowledgments

GEB, SMI and SEM were supported by the Natural Environment Research Council (NERC), UK, Grant NE/W006766/1. For the ground magnetometer data we gratefully acknowledge: INTERMAGNET (INTERMAGNET Operations Committee & INTERMAGNET Executive Council, 2024), Alan Thomson; CARISMA, PI Ian Mann; CANMOS, Geomagnetism Unit of the Geological Survey of Canada; The S-RAMP Database, PI K. Yumoto and Dr. K. Shiokawa; The SPIDR database; AARI, PI Oleg Troshichev; The MACCS program, PI M. Engebretson; GIMA; MEASURE, UCLA IGPP and Florida Institute of Technology; SAMBA, PI Eftyhia Zesta; 210 Chain, PI K. Yumoto; SAMNET, PI Farideh Honary; IMAGE, PI Liisa Juusola; Finnish Meteorological Institute, PI Liisa Juusola; Sodankyla Geophysical Observatory, PI Tero Raita; UiT the Arctic University of Norway, Tromsø Geophysical Observatory, PI Magnar G. Johnsen; GFZ German Research Centre For Geosciences, PI Jurgen Matzka; Institute of Geophysics, Polish Academy ofSciences, PI Anne Neska and Jan Reda; Polar Geophysical Institute, PI Alexander Yahnin and Yarolav Sakharov; Geological Survey of Sweden, PI Gerhard Schwarz; Swedish Institute of Space Physics, PI Masatoshi Yamauchi; AUTUMN, PI Martin Connors; DTU Space, Thom Edwards and PI Anna Willer; South Pole and McMurdo Magnetometer, PI's Louis J. Lanzarotti and Alan T. Weatherwax; ICESTAR; RAPIDMAG; British Artarctic Survey; McMac, PI Dr. Peter Chi; BGS, PI Dr. Susan Macmillan; Pushkov Institute of Terrestrial Magnetism, Ionosphere and Radio Wave Propagation (IZMIRAN); MFGI, PI B. Heilig; Institute of Geophysics, Polish Academy of Sciences, PI Anne Neska and Jan Reda; University of L'Aquila, PI M. Vellante; BCMT, V. Lesur and A. Chambodut; Data obtained in cooperation with Geoscience Australia, PI Andrew Lewis; AALPIP, co-PIs Bob Clauer and Michael Hartinger; MagStar, PI Jennifer Gannon; LISN PI Cesar Valladares; SuperMAG, PI Jesper W. Gjerloev; Data obtained in cooperation with the Australian Bureau of Meteorology, PI Richard Marshall. We acknowledge use of NASA/GSFC's Space Physics Data Facility's CDAWeb service (at http://cdaweb.gsfc.nasa.gov) and OMNI data. We acknowledge NASA contract NAS5-02099 and

References

Albertson, V. D., Thorson, J. M., Clayton, R. E., & Tripathy, S. C. (1973). Solar-induced-currents in power systems: Cause and effects. *IEEE Transactions on Power Apparatus and Systems*(2), 471–477. https://doi.org/10.1109/TPAS.1973.293746

Allen, J., Sauer, H., Frank, L., & Reiff, P. (1989). Effects of the March 1989 solar activity. *EOS Transactions of the American Geophysical Union*, *70*(46), 1479–1488. https://doi.org/10.1029/89EO00409

Bolduc, L. (2002). GIC observations and studies in the Hydro-Québec power system. *Journal of Atmospheric and Solar-Terrestrial Physics*, *64*(16), 1793–1802. https://doi.org/10.1016/S1364-6826(02)00128-1

Boteler, D., Pirjola, R., & Nevanlinna, H. (1998). The effects of geomagnetic disturbances on electrical systems at the earth's surface. *Advances in Space Research*, *22*(1), 17–27. https://doi.org/10.1016/S0273-1177(97)01096-X

Boteler, D. H. (2001). Space weather effects on power systems. *Geophysical Monograph-American Geophysical Union*, *125*, 347–352. https://doi.org/10.1029/GM125p0347

Bower, G., Imber, S., Milan, S., Schillings, A. L., Aand, F., & Gjerloev, J. (2024). Location of geomagnetic disturbances in relation to the field aligned current boundary. *Journal of Geophysical Research: Space Physics*, *129*(10), e2024JA033039. https://doi.org/10.1029/2024JA033039

Bower, G., Milan, S., Imber, S., Schillings, A., Fleetham, A., Beggan, C., & Gjerloev, J. (2025). Asymmetry in the ring current during geomagnetic disturbances. *Journal of Geophysical Research: Space Physics*, *130*(3), e2024JA033492. https://doi.org/10.1029/2024JA033492

Campbell, W. H. (1978). Induction of auroral zone electric currents within the Alaska pipeline. *Pure and Applied Geophysics*, *116*(6), 1143–1173. https://doi.org/10.1007/BF00874677

Carter, B. A., Yizengaw, E., Pradipta, R., Weygand, J. M., Piersanti, M., Pulkkinen, A., et al. (2016). Geomagnetically induced currents around the world during the 17 March 2015 storm. *Journal of Geophysical Research: Space Physics*, *121*(10), 10–496. https://doi.org/10.1002/2016JA023344

Clarke, E., Baillie, O., J. Reay, S., & Turbitt, C. W. (2013). A method for the near real-time production of quasi-definitive magnetic observatory data. *Earth Planets and Space*, *65*(11), 1363–1374. https://doi.org/10.5047/eps.2013.10.001

Donovan, E., Mende, S., Jackel, B., Frey, H., Syrjäsuo, M., Voronkov, I., et al. (2006). The THEMIS All-Sky Imaging array—system design and initial results from the prototype imager. *Journal of Atmospheric and Solar-Terrestrial Physics*, *68*(13), 1472–1487. https://doi.org/10.1016/j.jastp.2005.03.027

EPRI. (2020). Furthering the understanding of the characteristics and scales of geoelectric field enhancements. Techincal Report. 3002017900. EPRI.

Fleetham, A., Milan, S., Imber, S., Bower, G., Gjerloev, J., & Vines, S. (2024). The relationship between large dB/dt and field-aligned currents during five geomagnetic storms. *Journal of Geophysical Research: Space Physics*, *129*(7), e2024JA032483. https://doi.org/10.1029/2024JA032483

Freeman, M. P., Forsyth, C., & Rae, I. J. (2019). The influence of substorms on extreme rates of change of the surface horizontal magnetic field in the United Kingdom. *Space Weather*, *17*(6), 827–844. https://doi.org/10.1029/2018SW002148

Gaunt, C., & Coetzee, G. (2007). Transformer failures in regions incorrectly considered to have low GIC-risk. In *2007 IEEE Lausanne power tech* (pp. 807–812). https://doi.org/10.1109/PCT.2007.4538419

Gjerloev, J. W. (2012). The superMAG data processing technique. *Journal of Geophysical Research*, *117*(A9). https://doi.org/10.1029/2012JA017683

Grawe, M. A., Makela, J. J., Butala, M. D., & Kamalabadi, F. (2018). The impact of magnetic field temporal sampling on modeled surface electric fields. *Space Weather*, *16*(11), 1721–1739. https://doi.org/10.1029/2018SW001896

Grono, E., & Donovan, E. (2020). Surveying pulsating auroras. *Annales Geophysicae*, *38*, 1–8. https://doi.org/10.5194/angeo-38-1-2020

Hajra, R., Tsurutani, B. T., Lakhina, G. S., Lu, Q., & Du, A. (2024). Interplanetary causes and impacts of the May superstorm on the geosphere: An overview. *The Astrophysical Journal*, *974*(2), 264. https://doi.org/10.3847/1538-4357/ad7462

Hartinger, M. D., Shi, X., Rodger, C. J., Fujii, I., Rigler, E. J., Kappler, K., et al. (2023). Determining ulf wave contributions to geomagnetically induced currents: The important role of sampling rate. *Space Weather*, *21*(5), e2022SW003340. https://doi.org/10.1029/2022SW003340

Heyns, M. J., Lotz, S. I., & Gaunt, C. T. (2021). Geomagnetic pulsations driving geomagnetically induced currents. *Space Weather*, *19*(2), e2020SW002557. https://doi.org/10.1029/2020SW002557

Hübert, J., Beggan, C., Richardson, G., Gomez-Perez, N., Collins, A., & Thomson, A. (2024). Validating a UK geomagnetically induced current model using differential magnetometer measurements. *Space Weather*, *22*(2), e2023SW003769. https://doi.org/10.1029/2023SW003769

Hughes, J., Mcgranaghan, R., Kellerman, A. C., Bortnik, J., Arrit, R. F., Venkataramani, K., et al. (2022). Revealing novel connections between space weather and the power grid: Network analysis of ground-based magnetometer and geomagnetically induced currents (GIC) measurements. *Space Weather*, *20*(2), e2021SW002727. https://doi.org/10.1029/2021SW002727

INTERMAGNET Operations Committee, & INTERMAGNET Executive Council. (2024). Intermagnet Reference Data Set (IRDS) 2020 – Definitive Magnetic Observatory Data [Dataset]. *GFZ Data Services*. https://doi.org/10.5880/INTERMAGNET.1991.2020

Johnstone, A. (1978). Pulsating aurora. *Nature*, *274*(5667), 119–126. https://doi.org/10.1038/274119a0

Jones, S., Lessard, M., Rychert, K., Spanswick, E., & Donovan, E. (2011). Large-scale aspects and temporal evolution of pulsating aurora. *Journal of Geophysical Research*, *116*(A3). https://doi.org/10.1029/2010JA015840

Juusola, L., Viljanen, A., Van De Kamp, M., Tanskanen, E. I., Vanhamäki, H., Partamies, N., & Kauristie, K. (2015). High-latitude ionospheric equivalent currents during strong space storms: Regional perspective. *Space Weather*, *13*(1), 49–60. https://doi.org/10.1002/2014SW001139

Kataoka, R., & Ngwira, C. (2016). Extreme geomagnetically induced currents. *Progress in Earth and Planetary Science*, *3*, 1–7. https://doi.org/10.1186/s40645-016-0101-x

King, J. H., & Papitashvili, N. E. (2005). Solar wind spatial scales in and comparisons of hourly Wind and ACE plasma and magnetic field data. *Journal of Geophysical Research*, *110*(A2). https://doi.org/10.1029/2004JA010649

V. Angelopoulos for use of data from the THEMIS Mission. Specifically:S. Mende and E. Donovan for use of the ASI data, the CSA for logistical support in fielding and data retrieval from the GBO stations, and NSF for support of GIMNAST through Grant AGS-1004736. This research used the ALICE High Performance Computing facility at the University of Leicester. For the purpose of open access, the author has applied a Creative Commons Attribution (CC BY) license to the Author Accepted Manuscript version arising from this submission.

Lawrence, E., Beggan, C., Richardson, G., Reay, S., Thompson, V., Clarke, E., et al. (2025). The geomagnetic and geoelectric response to the May 2024 geomagnetic storm in the United Kingdom. *Frontiers in Astronomy and Space Sciences*, *12*, 1550923. https://doi.org/10.3389/fspas.2025.1550923

Lessard, M. (2012). A review of pulsating aurora. *Auroral phenomenology and magnetospheric processes: Earth and other planets*, *197*, 55–68. https://doi.org/10.1029/2011GM001187

Liou, K., Newell, P., Sibeck, D., Meng, C.-I., Brittnacher, M., & Parks, G. (2001). Observation of IMF and seasonal effects in the location of auroral substorm onset. *Journal of Geophysical Research*, *106*(A4), 5799–5810. https://doi.org/10.1029/2000JA003001

Macmillan, S., & Olsen, N. (2013). Observatory data and the Swarm mission. *Earth Planets and Space*, *65*(11), 1355–1362. https://doi.org/10.5047/eps.2013.07.011

Marshall, R. A., Dalzell, M., Waters, C. L., Goldthorpe, P., & Smith, E. A. (2012). Geomagnetically induced currents in the New Zealand power network. *Space Weather*, *10*(8). https://doi.org/10.1029/2012SW000806

Marshall, R. A., Waters, C. L., & Sciffer, M. D. (2010). Spectral analysis of pipe-to-soil potentials with variations of the Earth's magnetic field in the Australian region. *Space Weather*, *8*(5). https://doi.org/10.1029/2009SW000553

Milan, S., Bower, G., Fleetham, A., Imber, S., Schillings, A., Opgenoorth, H., et al. (2024). Occurrence and causes of large dB/dt events and AL bays in the pre-midnight and dawn sectors. *Journal of Geophysical Research: Space Physics*, *129*(10), e2024JA032811. https://doi.org/10.1029/2024JA032811

Milan, S., Carter, J., Sangha, H., Bower, G., & Anderson, B. (2021). Magnetospheric flux throughput in the Dungey cycle: Identification of convection state during 2010. *Journal of Geophysical Research: Space Physics*, *126*(2), e2020JA028437. https://doi.org/10.1029/2020JA028437

Milan, S., Imber, S., Fleetham, A., & Gjerloev, J. (2023). Solar cycle and solar wind dependence of the occurrence of large dB/dt events at high latitudes. *Journal of Geophysical Research: Space Physics*, *128*(4), e2022JA030953. https://doi.org/10.1029/2022JA030953

Molinski, T. S., Feero, W. E., & Damsky, B. L. (2000). Shielding grids from solar storms [power system protection]. *IEEE Spectrum*, *37*(11), 55–60. https://doi.org/10.1109/6.880955

Newell, P., & Gjerloev, J. (2012). SuperMAG-based partial ring current indices. *Journal of Geophysical Research*, *117*(A5). https://doi.org/10.1029/2012JA017586

Ngwira, C. M., Pulkkinen, A., Wilder, F. D., & Crowley, G. (2013). Extended study of extreme geoelectric field event scenarios for geomagnetically induced current applications. *Space Weather*, *11*(3), 121–131. https://doi.org/10.1002/swe.20021

Ohtani, S., Gjerloev, J. W., Anderson, B. J., Kataoka, R., Troshichev, O., & Watari, S. (2018). Dawnside wedge current system formed during intense geomagnetic storms. *Journal of Geophysical Research: Space Physics*, *123*(11), 9093–9109. https://doi.org/10.1029/2018JA025678

Orr, L., Chapman, S. C., & Beggan, C. D. (2021). Wavelet and network analysis of magnetic field variation and geomagnetically induced currents during large storms. *Space Weather*, *19*(9), e2021SW002772. https://doi.org/10.1029/2021SW002772

Partamies, N., Weygand, J. M., & Juusola, L. (2017). Statistical study of auroral omega bands. *Annales Geophysicae*, *35*(5), 1069–1083. https://doi.org/10.5194/angeo-35-1069-2017

Pulkkinen, A., Bernabeu, E., Eichner, J., Beggan, C., & Thomson, A. (2012). Generation of 100-year geomagnetically induced current scenarios. *Space Weather*, *10*(4). https://doi.org/10.1029/2011SW000750

Pulkkinen, A., Pirjola, R., & Viljanen, A. (2008). Statistics of extreme geomagnetically induced current events. *Space Weather*, *6*(7). https://doi.org/10.1029/2008SW000388

Rodger, C. J., Mac Manus, D. H., Dalzell, M., Thomson, A. W., Clarke, E., Petersen, T., et al. (2017). Long-term geomagnetically induced current observations from New Zealand: Peak current estimates for extreme geomagnetic storms. *Space Weather*, *15*(11), 1447–1460. https://doi.org/10.1002/2017SW001691

Rogers, N. C., Wild, J. A., Eastoe, E., & Huebert, J. (2021). Climatological statistics of extreme geomagnetic fluctuations with periods from 1 s to 60 min. *Space Weather*, *19*(11), e2021SW002824. https://doi.org/10.1029/2021SW002824

Royrvik, O., & Davis, T. (1977). Pulsating aurora: Local and global morphology. *Journal of Geophysical Research*, *82*(29), 4720–4740. https://doi.org/10.1029/JA082i029p04720

Schillings, A., Palin, L., Opgenoorth, H. J., Hamrin, M., Rosenqvist, L., Gjerloev, J. W., et al. (2022). Distribution and occurrence frequency of dB/dt spikes during magnetic storms 1980–2020. *Space Weather*, *20*(5), e2021SW002953. https://doi.org/10.1029/2021SW002953

Smith, A., Rodger, C., Pratscher, K., Mac Manus, D., Rae, I., Ratliff, D., et al. (2025). Why do sudden commencements sometimes generate disproportionate geomagnetically induced currents? *Space Weather*, *23*(10), e2025SW004533. https://doi.org/10.1029/2025SW004533

Sokolova, O., Burgherr, P., Sakharov, Y., & Korovkin, N. (2018). Algorithm for analysis of power grid vulnerability to geomagnetic disturbances. *Space Weather*, *16*(10), 1570–1582. https://doi.org/10.1029/2018SW001931

Sorathia, K., Merkin, V. G., Ohtani, S., Keesee, A. M., Michael, A., Sciola, A., et al. (2022). Multiscale magnetosphere-ionosphere coupling during stormtime: A case study of the dawnside current wedge. *Agu fall meeting abstracts*, *2022*(11), SM42E–2224. https://doi.org/10.1029/2023JA031594

SuperMAG. (2023a). Supermag data. SuperMAG portal [Dataset]. Retrieved from https://supermag.jhuapl.edu/mag/?fidelity=high

SuperMAG. (2023b). SuperMAG data. SuperMAG portal [Dataset]. Retrieved from https://supermag.jhuapl.edu/mag/?fidelity=low

Tanskanen, E., Pulkkinen, T., Koskinen, H., & Slavin, J. (2002). Substorm energy budget during low and high solar activity: 1997 and 1999 compared. *Journal of Geophysical Research*, *107*(A6), SMP–15. https://doi.org/10.1029/2001JA900153

Trichtchenko, L. (2021). Frequency considerations in gic applications. *Space Weather*, *19*(8), e2020SW002694. https://doi.org/10.1029/2020SW002694

Viljanen, A. (1997). The relation between geomagnetic variations and their time derivatives and implications for estimation of induction risks. *Geophysical Research Letters*, *24*(6), 631–634. https://doi.org/10.1029/97GL00538

Viljanen, A., Nevanlinna, H., Pajunpää, K., & Pulkkinen, A. (2001). Time derivative of the horizontal geomagnetic field as an activity indicator. *Annales Geophysicae*, *19*(9), 1107–1118. https://doi.org/10.5194/angeo-19-1107-2001

Viljanen, A., & Tanskanen, E. (2013). High-latitude magnetic fields and their time derivatives: Interhemispheric similarities. *Earth Planets and Space*, *65*(1), 45–49. https://doi.org/10.5047/eps.2012.05.014

Vokhmyanin, M., Apatenkov, S., Gordeev, E., Andreeva, V., Partamies, N., Kauristie, K., & Juusola, L. (2021). Statistics on omega band properties and related geomagnetic variations. *Journal of Geophysical Research: Space Physics*, *126*(7), e2021JA029468. https://doi.org/10.1029/2021JA029468

Watari, S., Nakamura, S., & Ebihara, Y. (2021). *Measurement of geomagnetically induced current (GIC) around Tokyo, Japan (Tech. Rep.)*. Springer. https://doi.org/10.1186/s40623-021-01422-3

15427390, 2026, 6, Downloaded from https://agupubs.onlinelibrary.wiley.com/doi/10.1029/2026SW004959 by British Geological Survey, Wiley Online Library on [31/07/2026]. See the Terms and Conditions (https://onlinelibrary.wiley.com/terms-and-conditions) on Wiley Online Library for rules of use; OA articles are governed by the applicable Creative Commons License

Weigel, R. S., Vassiliadis, D., & Klimas, A. J. (2002). Coupling of the solar wind to temporal fluctuations in ground magnetic fields. *Geophysical Research Letters*, *29*(19), 21–1. https://doi.org/10.1029/2002GL014740

Yang, B., Donovan, E., Liang, J., & Spanswick, E. (2017). A statistical study of the motion of pulsating aurora patches: Using the THEMIS All-sky imager. *Annales Geophysicae*, *35*(2), 217–225. https://doi.org/10.5194/angeo-35-217-2017

Zou, Y., Dowell, C., Ferdousi, B., Lyons, L. R., & Liu, J. (2022). Auroral drivers of large dB/dt during geomagnetic storms. *Space Weather*, *20*(11), e2022SW003121. https://doi.org/10.1029/2022SW003121

15427390, 2026, 6, Downloaded from https://agupubs.onlinelibrary.wiley.com/doi/10.1029/2026SW004959 by British Geological Survey, Wiley Online Library on [31/07/2026]. See the Terms and Conditions (https://onlinelibrary.wiley.com/terms-and-conditions) on Wiley Online Library for rules of use; OA articles are governed by the applicable Creative Commons License